Soft Matter

PAPER

View Article Online
View Journal | View Issue

Cite this: *Soft Matter*, 2022, **18**, 9216

Crystallization and molecular mobility in renewable semicrystalline copolymers based on polycaprolactone and polyisosorbide†

Chaima Bouyahya,[ab] Nikolaos D. Bikiaris,[a] Alexandra Zamboulis,[a] Apostolos Kyritsis,[c] Mustapha Majdoub*[b] and Panagiotis A. Klonos*[ac]

A series of novel block copolymers based on two biodegradable polymers, poly(ε-caprolactone), PCL, and poly(isosorbide), PIS, with PIS fractions 5, 10, and 25 wt%, are studied herein. The aim is to assess the effects of the amorphous PIS phase on the properties of the semicrystalline PCL (majority), in addition to the synthesis strategy. The latter involved the polymerization of caprolactone onto initial PIS of low molar mass, resulting, thus, in gradually shorter PCL blocks when the starting amount of PIS is increased. The structure–property relationship investigation, with an emphasis on molecular mobility and crystallization, involves the following sum of complementary techniques: differential scanning calorimetry, dielectric spectroscopy, polarized optical microscopy and X-ray diffraction. The molecular mobility map for these PCL/PIS and initial PIS is drawn here for the first time. Despite the high glass transition temperature of PIS (T_g ~ 51 °C) compared to that of PCL (−66 °C), the T_g of the copolymers barely changes, as it is mainly ruled by crystallinity. The latter seems to be facilitated in the copolymers, in both the amount and the rate. The local molecular mobility of PCL and PCL/PIS consists of faster γ_{PCL} relaxation which is unaffected in the copolymers, whereas the slower β_{PCL} process arising from the backbone ester group rotation exhibits a systematic deceleration in the presence of PIS. A connection between such local motions and the corresponding segmental α relaxation, observed previously in other polyesters, is also found to be true here. Apart from that, the dielectric T_g as well as the cooperativity of the polymer chains drop moderately, which indicates spatial confinement between the PCL crystals, whereas correlations with the looser lamellar chain packing within the spherulites are gained. The relaxations of initial PIS, *i.e.*, γ_{PIS}, β_{PIS} and α_{PIS}, could not be resolved within the copolymers. Along with other properties, such as ionic conductivity, we conclude to the homogeneity of our systems, with sufficient PCL/PIS distribution.

Received 5th September 2022,
Accepted 9th November 2022

DOI: 10.1039/d2sm01198k

rsc.li/soft-matter-journal

1. Introduction

Synthetic polymers have been improving our everyday life for more than a century now[1–3] and nowadays plastics are found everywhere: in our homes, transport, buildings, healthcare, *etc.* Polymeric materials owe their success to their unique properties; indeed, they are high performance materials, which are easily processed and have a low cost of production.[2] However, numerous concerns are being raised regarding the oil-based origin of most polymers and their accumulation in the environment due to their lack of degradability.[4–7] Plastics are increasingly perceived as non-eco-friendly materials by the wider public, overestimating their actual contribution to the environmental crisis. These concerns have driven the advent of the field of biobased polymers, *i.e.*, polymers synthesized from renewable resources, the polylactide family being the most commercially viable for the time being.[8–13] To widen the portfolio of biobased polymers and, thus their potential applications, intensive research in the field is being conducted, both by academia and industry.[14,15] Several other polyesters, both aliphatic ones such as poly(*n*-alkylene succinate)s[16,17] and glycerol-based polyesters,[18] as well as aromatic ones, furanoate polyesters, produced from 2,5-furan-dicarboxylic acid,[19,20] and polyvanillates,[21] are being investigated. In addition to good performance, renewability and biocompatibility, such materials serve well within the circular

[a] *Department of Chemistry, Laboratory of Polymer Chemistry and Technology, Aristotle University of Thessaloniki, GR-541 24, Thessaloniki, Greece. E-mail: pklonos@central.ntua.gr*
[b] *Laboratoire des Interfaces et Matériaux Avancés, Université de Monastir, 5000 Monastir, Tunisia. E-mail: mustapha.majdoub@fsm.rnu.tn*
[c] *Department of Physics, National Technical University of Athens, Zografou Campus, 15780, Athens, Greece*

† Electronic supplementary information (ESI) available. See DOI: https://doi.org/10.1039/d2sm01198k

and the green economic prescripts.[22,23] Moreover, copolymers, blends and composites of biobased polymers[24–32] are being developed to further improve the properties and performance of these promising polymers.[33,34]

Isosorbide is a V-shaped diol that carries two sterically different secondary hydroxyl groups, with the so-called '*exo*-' and '*endo*-' configurations, respectively, and two '*cis*-' connected tetrahydrofuran rings.[35,36] It is a commercially available biobased monomer, produced from D-glucose (on the industrial scale) or starch.[36] This non-toxic chiral diol has been employed for the stepwise development of various polymers, including polyesters, polyurethanes, polyamides, polycarbonates, *etc.*[37–40] In the context of the present study, we will discuss poly(isosorbide), PIS, which is an isosorbide-based poly(acetal).[41,42] PIS is an amorphous polymer with a T_g of around 50 °C. PIS has two pending hydroxyl groups and its copolymerization with other aliphatic polymers could contribute to the increase in their rigidity and phase-transition temperatures. Herein, we have combined PIS with poly(ε-caprolactone) (PCL).

PCL is a biocompatible (non-toxic) and hydrophobic polyester,[43] that is characterized by a slow *in vivo* hydrolysis.[44] It is generally synthesized by the ring-opening polymerization (ROP) of ε-caprolactone.[45,46] PCL demonstrates quite good mechanical performance and permeation (gas barrier) characteristics, but relatively low glass transition temperatures (far below room temperature) and mild melting points (~60 °C).[43] Since this polyester is semicrystalline, with a high degree of crystallinity (mainly 50% and larger),[30,43,47,48] its performance is strongly connected with crystallinity. As a consequence, its permeation to small molecules (air, humidity),[49] heat transport and mechanical strength[50,51] depends on the semicrystalline morphology (size, numbers and distributions of polymer crystals).[52,53] In connection to that, PCL demonstrates a pronounced phenomenon of 'crystal/nucleation memory'[48,54,55] that plays a key role in manipulating the semicrystalline morphology by appropriately chosen thermal protocols (melting temperature, supercooling, *etc.*). Crystal memory, nucleation and lamella packing depend also on the macromolecular chain mobility, chain–chain organization, interchain interactions and reactivity.[56–58]

As already mentioned, the materials' performance can be further tuned by combining one polymer with another. PCL has been widely demonstrated to show almost unique compatibility with various polymers.[59] PCL co-polyesters of various forms, from linear blocks to star-shaped and hyperbranched copolymers, can be synthesized employing either multifunctional comonomers or oligomers.[18,50,60–62]

For the present study, we have combined PCL with a newer biobased polymer, *i.e.*, poly(isosorbide) (PIS). PIS is produced from starch, or, on the industrial scale, from D-glucose.[36] Isosorbide is a V-shaped diol that carries two sterically different secondary hydroxyl groups, with the so-called '*exo*-' and '*endo*-' configurations, respectively, and two '*cis*-' connected tetrahydrofuran rings.[35,36] This non-toxic chiral diol has been employed within various synthetic processes for the step-development of various polymers, including polyesters, polyurethanes, polyamides, polycarbonates, *etc.*[35,38–40]

Herein, PIS of relatively small molar mass (short length) was used, *via* its hydroxyl groups (–OH), as a macro-initiator for the ROP of ε-caprolactone, yielding copolymers with PIS and PCL blocks. We have synthesized three diblock copolymers, namely, with different PCL/PIS wt% ratios of 95/5, 90/10 and 75/25, which are studied and compared with neat PCL and initial PIS. The focus here is on the direct and indirect effects of block copolymer composition and chain length on the glass transition, crystallization and finally on the local and segmental mobility. The investigation involves a series of complementary techniques, differential scanning calorimetry (DSC), polarized optical microscopy (POM), X-ray diffraction (XRD), combined with the technique of broadband dielectric spectroscopy (BDS).[63] To the best of our knowledge, the molecular mobility for these PCL/PIS systems and PIS individually is shown for the first time.

2. Materials and experimental techniques

2.1 Materials – preparation of PCL/PIS copolymers

PIS was synthesized according to a previously reported method with some modifications.[42] Briefly, a stirred mixture of isosorbide and potassium hydroxide powder in a small amount of dimethyl sulfoxide was purged with argon. Then, an excess of methylene chloride was gradually added, and the reaction mixture was kept under magnetic stirring at room temperature for 120 h. The polymer obtained was precipitated in methanol and dried under vacuum.

Three PCL-*b*-PIS copolymer samples were synthesized by the ROP of ε-caprolactone[64,65] in the presence of the pre-synthesized low molar mass, M_n ~ 15 kg mol^{-1} PIS (Fig. 1). PIS exhibits terminal –OH sites, onto which the building of PCL block takes place, in accordance also with previous works on PCL[58] and other polyesters.[66] The PCL(%)/PIS(%) ratios have been chosen here as 95/5, 90/10 and 74/25. To facilitate a direct comparison with copolymers with neat polymers, we synthesized neat –OH terminated PCL, again by ROP. The latter is studied in parallel with the copolymers and initial PIS. Due to the method of copolymer synthesis, we expect a decrease in the average molar mass (chain length, bottom of Fig. 1) with the increase of the PIS fraction, as the number of ROP initiation points increases.[58,66,67] This was confirmed by the intrinsic viscosity, $[\eta]$, which drops from 0.78 dL g^{-1} in PCL to 0.48, 0.36 and 0.28 dL g^{-1}, for 5%, 10% and 20% PIS, respectively. According to gel permeation chromatography, M_n is ~90 kg mol^{-1} in neat PCL and drops gradually to ~12 kg mol^{-1} in PCL(75%)-*b*-PIS(25%). Please note that $[\eta]$ of the initial PIS was 0.32 dL g^{-1}. The prepared samples were placed in a homemade mold, thermally pressed and finally, received in the form of disks ~1.8 mm in thickness and 25 mm in diameter.

2.2. Characterization methods

DSC was employed to investigate the polymers' thermal transitions. The measurements were performed under a high purity helium atmosphere (99.9995%), on samples 8–9 mg in mass

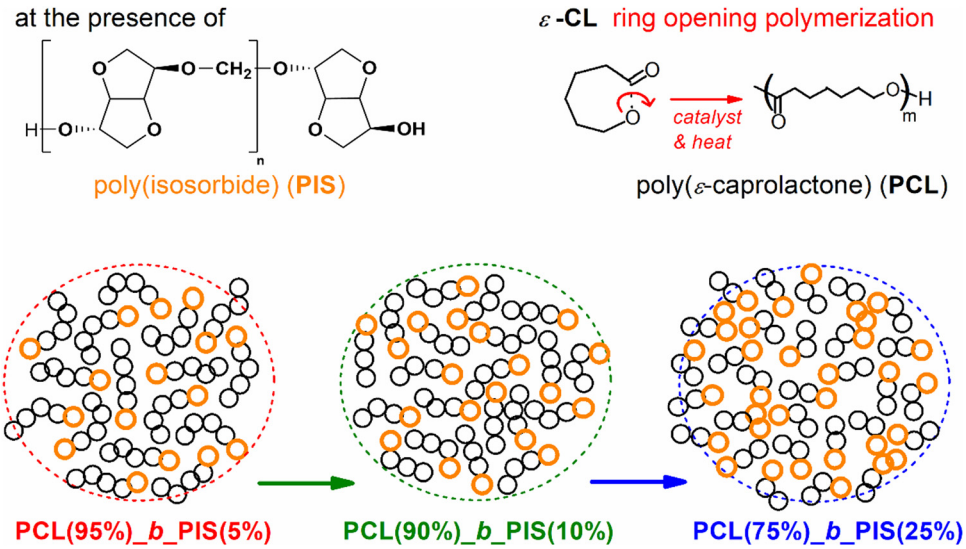

Fig. 1 Schematic view of PCL/PIS copolymer preparation, *via* ROP and building of PCL blocks on existing PIS segments.

sealed in TZero aluminium pans and within the temperature range from −150 to 100 °C, by means of a TA Q200 DSC apparatus (TA Instruments, USA) equipped with a liquid nitrogen control system (LNCS). The instrument had been previously calibrated with indium for temperature and enthalpy and sapphires for heat capacity. The cooling/heating profiles are shown in Scheme 1. Upon erasing the thermal history *via* a first heating scan up to 100 °C at 10 K min^{-1} (scan 1), all samples were cooled down to −150 at 20 K min^{-1} (scan 2) and, in another scan, at the fastest achievable rate ('jump' command of the TA software, scan 3). The latter resulted in a non-constant cooling rate, being ∼90 K min^{-1} (Scheme 1b) on average in the temperature range of PCL's crystallization. The employment of different cooling rates for scans 2 and 3 aims at the manipulation of crystallization, for example, to be suppressed during fast cooling or facilitated during slower cooling. The subsequent heating scans up to 100 °C were performed at a fixed rate of 10 K min^{-1} (Scheme 1).

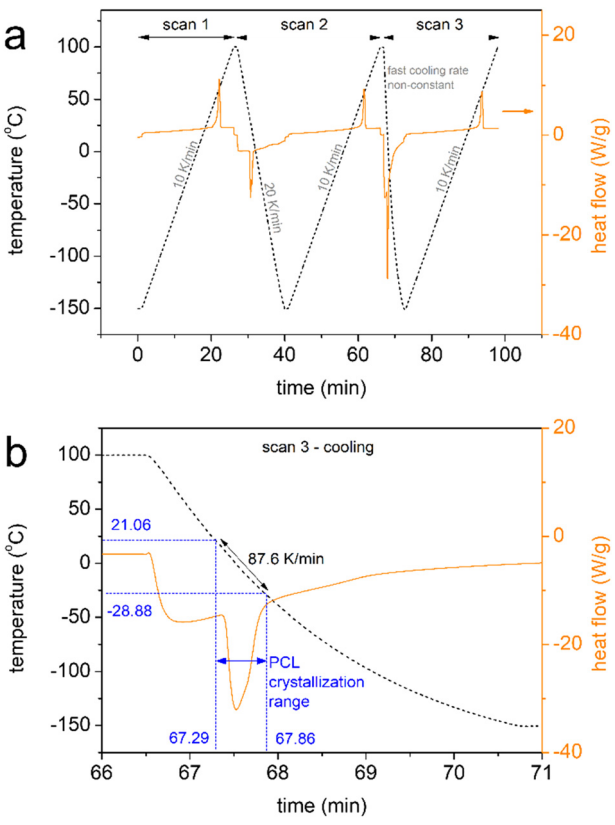

Scheme 1 (a) The time–temperature profiles during scans 1–3 of the DSC measurements. (b) The time–temperature profile of the relatively fast cooling during scan 3. A rough estimation of the cooling rate is supplied in (b) in the temperature range of PCL's crystallization.

The crystalline fraction, CF, was estimated by both crystallization and melting peaks in DSC, by comparing the crystallization enthalpy (ΔH_c and ΔH_m, respectively) with the theoretical heat of fusion for a 100% crystalline PCL, $\Delta H_{100\%,PCL}$, taken as 139.5 J g^{-1},[68] according to eqn 1.

$$CF_{c/m} = \frac{\Delta H_{c/m}}{\Delta H_{100\%,PCL}} \quad (1)$$

To assess the semicrystalline structure, X-ray diffraction, XRD, was employed on samples that had been previously subjected to erased thermal history and cooled at 20 K min^{-1}. The diffraction spectra were recorded at room temperature employing a MiniFlex II XRD system (Rigaku Co., Japan), with Cu Ka radiation (λ = 0.154 nm), over a 2θ range from 5° to 50° with a scanning rate of 1 deg min^{-1}. Upon analysis of the diffraction peaks by mathematical models (Lorentzians), we were able to extract a rough estimation of the crystalline fraction, CF_{XRD},[67] by comparing the sum of crystalline peak areas, A_{cryst}, with the overall diffraction area, amorphous halos and crystalline peaks, '$A_{amorphous}$+ A_{cryst}' (eqn 2).

$$CF_{XRD} = \frac{A_{cryst}}{A_{overall}} = \frac{A_{cryst}}{A_{amorphous} + A_{cryst}} \quad (2)$$

Polarized optical microscopy, POM, images of the semicrystalline morphology for all PCL-based systems, during the

evolution of crystallization from the melt state and upon cooling at ~10 K min^{-1} (the actual time–temperature profile can be seen in section S1 of the ESI†), were recorded by means of a Nikon Optiphot-1 polarizing microscope equipped with a Linkam THMS 600 heated stage, a Linkam TP91 control unit and a Jenoptic ProgRes GRYPHAX® NAOS 20mp microscope camera.

To investigate molecular mobility in the copolymers and the corresponding effects of composition and compare with the molecular mobility of neat PCL and initial PIS, BDS was employed, a technique characterized by a quite high resolving power.[63] For that, a Novocontrol BDS setup was used, *i.e.*, an Alpha frequency response analyzer combined with a Quatro liquid nitrogen cryosystem (Novocontrol GmbH, Germany). Prior to the measurements, the samples were kept in a dry environment. Small pieces of ~50 mg in mass of the synthesized polymers were initially placed and melted at ~100 °C between finely polished brass electrodes of 14 mm diameter. To prevent the electrical contact of the electrodes and keep them parallel with each other, silica spacers of ~100 μm thickness by Novocontrol were used. Then, the complex dielectric permittivity (eqn 3),

$$\varepsilon^*(f, T) = \varepsilon'(f, T) - i\cdot\varepsilon''(f, T) \quad (3)$$

was recorded under a nitrogen atmosphere (N_2 gas flow), isothermally as a function of frequency, f, in the range from 10^{-1} to 10^6 Hz and in the temperature range between −150 and 120 °C, upon heating at steps of 5 and 10 K. The dielectric spectra, consisting of various contributions, were analysed by fitting appropriate models, mainly, the Havriliak–Negami, HN,[69] function (eqn 4),

$$\varepsilon^*(f) = \varepsilon_\infty + \frac{\Delta\varepsilon}{[1 + (if/f_0)^{\alpha_{HN}}]^{\beta_{HN}}} \quad (4)$$

wherein, ε_∞ describes the value of the real part of dielectric permittivity, ε', for $f \gg f_0$, $\Delta\varepsilon$ is the dielectric strength, f_0 is a characteristic frequency related to the frequency of maximum dielectric loss and α_{HN} and β_{HN} are shape parameters, for width and symmetry, respectively. The analysis process may be performed by different routes, for example, by the fitting of ε'' or ε', either individually or in parallel[70–72] (Fig. S2 in ESI†). Herein, we have chosen to fit $\varepsilon''(f)$. In this analysis, we constructed the time scale map of local and segmental relaxations. The local processes usually obey the Arrhenius equation[69] (eqn 5),

$$f(T) = f_{0,Arrh} \cdot e^{-\frac{E_{act}}{kT}} \quad (5)$$

as they exhibit a temperature-independent activation energy, E_{act}. On the other hand, the segmental relaxations, related to the glass transition, demonstrate a different time scale, usually described by the Vogel–Fulcher–Tammann–Hesse (VFTH) expression[69,73] (eqn 6),

$$f(T) = f_{0,VFTH} \cdot e^{-\frac{DT_0}{T-T_0}} \quad (6)$$

within which, D is the so-called fragility strength parameter[73] and is related to the measure of cooperativity, namely, the fragility index, m.

3. Results and discussion

To provide the first view of the thermal transitions of PCL, we show in Fig. 2 the corresponding DSC thermograms. In all cases, neat PCL exhibits a glass transition step, with the characteristic temperature, T_g= −66 °C. T_g seems independent of the rate of prior cooling, as during both slow and faster cooling, PCL crystallized at around 20–30 °C. The degree of crystallinity of neat PCL is CF_c = 0.32 wt (eqn 1).

We note that the employment of the highest cooling rate aimed at the elimination of crystallization and, thus, the production of 'amorphous' PCL. The latter was found impossible by such 'conventional' method, in accordance with previous works.[48,58,74]

We may now follow the effects imposed on the thermal events in the copolymers. In Fig. 3, results from scan 2 (cooling at 20 K min^{-1}, Fig. 3a, heating at 10 K min^{-1}, Fig. 3b) are shown, comparatively for all compositions and initial PIS.

Beginning from the melt state, during cooling (Fig. 3a), PCL exhibits a wide and double-structured crystallization exotherm. This probably correlates with multiple crystallization mechanisms of PCL.[54] All copolymers exhibit a single peak, located mainly at higher temperatures. The effect may originate from the favoring of one crystallization mechanism or, in other words, a more oriented crystallization. Such effects on crystallizability are often recorded in block copolymers.[75] This point can be further followed by specific experiments (isothermal crystallization, crystallization under various cooling rates, *etc.*) and corresponding analysis (*e.g.*, Avrami method).[75] The results are further evaluated and the values are listed in Table 1. Selected values have been plotted as a function of PIS fraction and are shown in Fig. 4. Therein, the crystallization temperature, T_c, tends to increase from 28 to 31 °C and so does CF_c, from 0.32 up to 0.48 wt (Fig. 4a). These are indications of the facilitation of

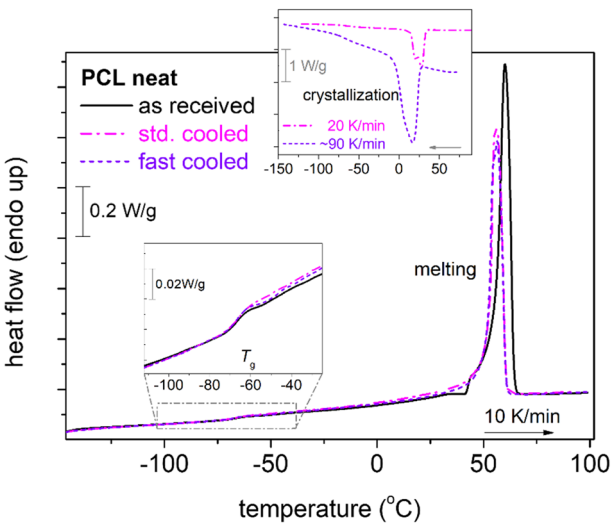

Fig. 2 Comparative DSC heating traces for neat PCL from the described thermal histories. The recorded heat flow (mW) is shown by normalization to the sample mass (W g^{-1}). The insets show in more detail the region of the glass transition steps as well as (inset on top) the recorded crystallization during prior cooling.

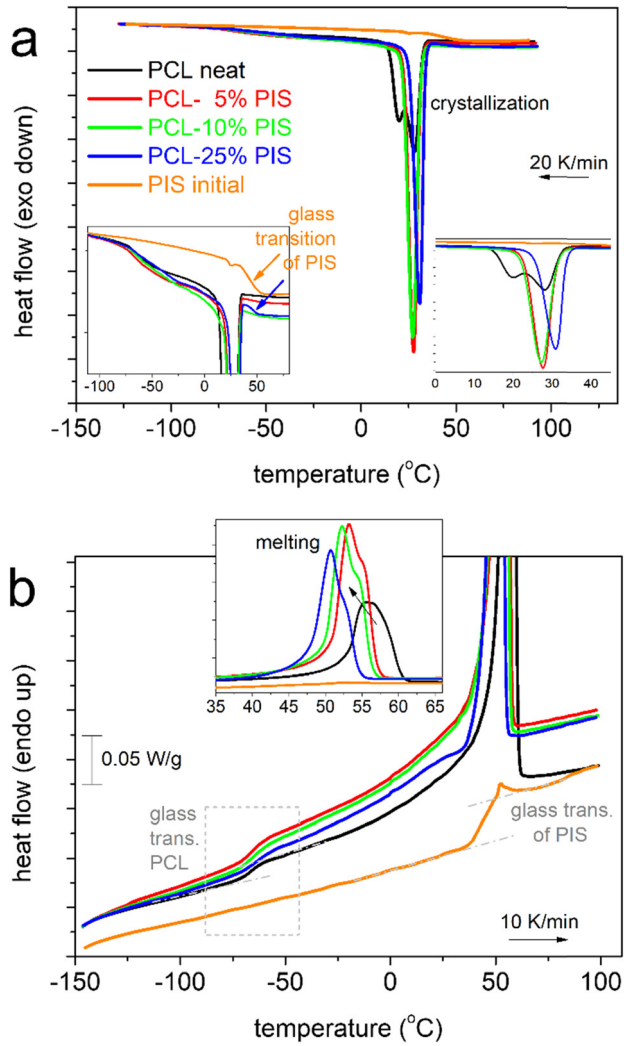

Fig. 3 DSC traces (a) during cooling at 20 K min^{-1} and (b) the subsequent heating at 10 K min^{-1} for all samples, copolymers and neat PCL and PIS. The main thermal events are marked on the plots. (b) Added dash-dotted lines corresponding to the measurement baselines prior and upon glass transition.

both the rate and the amount of crystallization, which seems to be more homogeneous (single-peaked) in the copolymers. Qualitatively similar results were revealed from scan 3, involving faster cooling (Fig. 5).

When estimating CF from melting, CF_m, and comparing with CF_c, we record a qualitative agreement in Fig. 4b. Then, we interestingly record a monotonic decrease in the melting temperature, T_m, from 56 down to 51 °C with increasing PIS. This could suggest the lowering of crystal quality in the copolymers, *e.g.*, in the chains' packing density, and correlate with the existence of PIS segments that act as defects in the copolymers.

Based on the overall data on crystallization, we expect mild alternations in the semicrystalline morphology, namely, on the size and distribution of PCL spherulites, whereas, stronger effects on the density of the crystals.

Coming to the chains' mobility, we follow the effects on glass transition. Individual T_g of initial PIS, which is amorphous, is 51 °C (Fig. 3b and 5b), whereas the corresponding heat capacity change is Δc_p = 0.26 J g^{-1} K^{-1}. Obviously, the polymer chain mobility within all the PCL-based systems will be ruled by the presence of crystals, thus, the direct chain copolymeric structure effects cannot be simply resolved. In Fig. 4c, T_g seems mainly unchanged, about −66 °C. With the exception of PCL(75%)-*b*-PIS(25%), we have no indication of separate glass transition of the PIS phase. Thus, for the rest of the copolymers, we expect homogeneous distribution of PCL_PIS blocks, with gradually shorter PCL segments on increasing PIS.[58,67,76] The shortening of the chain length should result in general in the lowering of the T_g. Most probably, this does not apply here, as the measured molar masses are above the value of 10 kg mol^{-1}, namely, all laying above the expected threshold for chain–chain entanglements. On the other hand, an increase in the number of free chain ends, *i.e.*, the number of free hydroxyls (–OH), is expected when the overall copolymer chain length decreases (Fig. 1). In turn, this should favor more chain–chain interactions, for example, between the hydroxyls and the ester groups (–C═O) of caprolactone. Taken individually, without considering the PCL chain shortening, the increased chain–chain interactions are expected to lead to higher T_g values. Therefore, we believe that the 'unchanged' T_g shown in Fig. 4c, is a result of compensation between the two effects described above along with the high crystalline fraction. It is worth noting that the said PCL interchain interactions have been proven to be responsible for the interesting crystal-memory effects exhibited in PCL[54,77] and studied by various techniques.[48]

In the insets to Fig. 3a and 5a, we follow that during cooling of PCL(75%)-*b*-PIS(25%), a step-like event is recorded at around 45 °C. From our data it is not clear as to whether such step exists within the copolymers with smaller PIS contents.

Table 1 Values of interest by DSC (scan 2): crystallization/melting temperatures, T_c/T_m, and enthalpies, ΔH_c/ΔH_m, crystalline fraction evaluated *via* the crystallization/melting peak, $CF_{c/m}$, glass transition temeperature, T_g, corresponding heat capacity change, Δc_p. Please note that the ΔH_i values are shown upon normalization to the PCL mass fraction, whereas, Δc_p values are shown upon normalization to the 'amorphous PCL' mass fraction, including also the crystalline fraction as estimated from XRD, CF_{XRD}

	T_c (°C)	$\Delta H_{c,n}$ (J g_{PCL}^{-1}) (±1)	CF_c (wt) (±0.01)	T_g (°C)	$\Delta c_{p,n}$ (J g_{am}^{-1} K^{-1})	T_m (°C)	$\Delta H_{m,n}$ (J g_{PCL}^{-1})	CF_m (wt) (±0.03)	CF_{XRD} (±0.05)
PCL (neat)	28/20	44	0.32	−66	0.16	56	49	0.35	0.33
PCL(95%)-*b*-PIS(5%)	28	63	0.45	−67	0.25	53	68	0.49	0.46
PCL(90%)-*b*-PIS(10%)	28	67	0.48	−66	0.33	52	72	0.52	0.49
PCL(75%)-*b*-PIS(25%)	31	63	0.45	−66	0.30	51	69	0.50	0.50
PIS (initial)	—	—	—	51	0.26	—	—	—	—

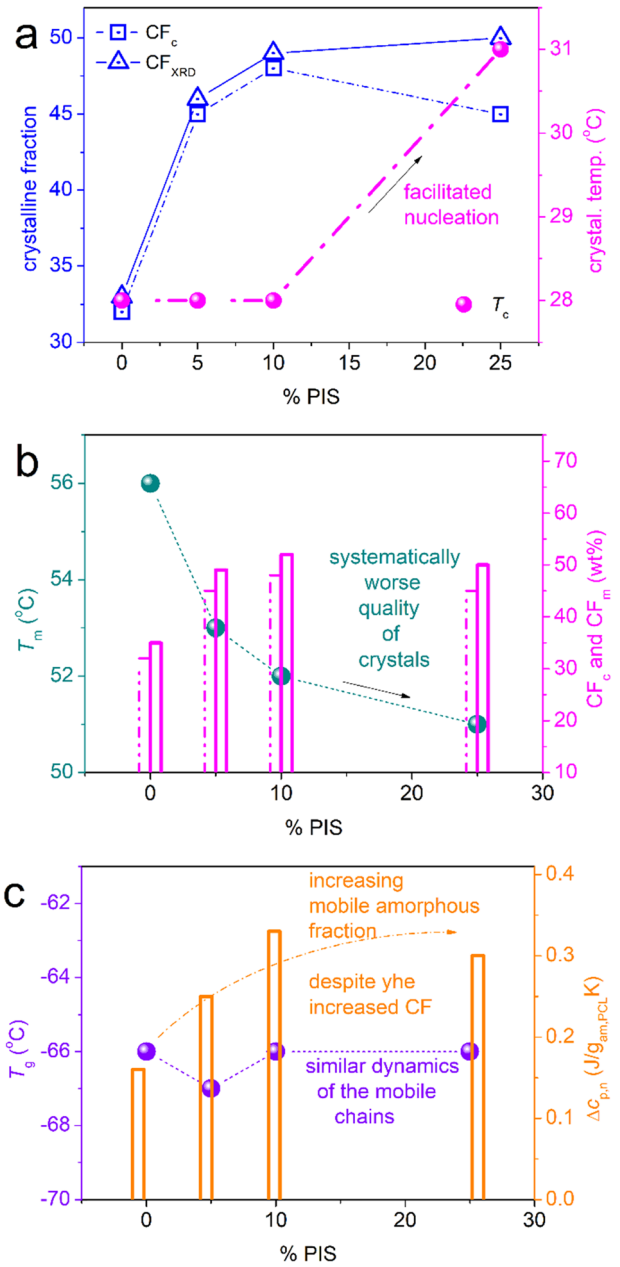

Fig. 4 The % PIS dependence of the thermal events assigned to PCL, namely, (a) crystallization temperature and crystalline fraction, (b) melting temperature and crystalline fraction and (c) glass transition temperature and the corresponding heat capacity change.

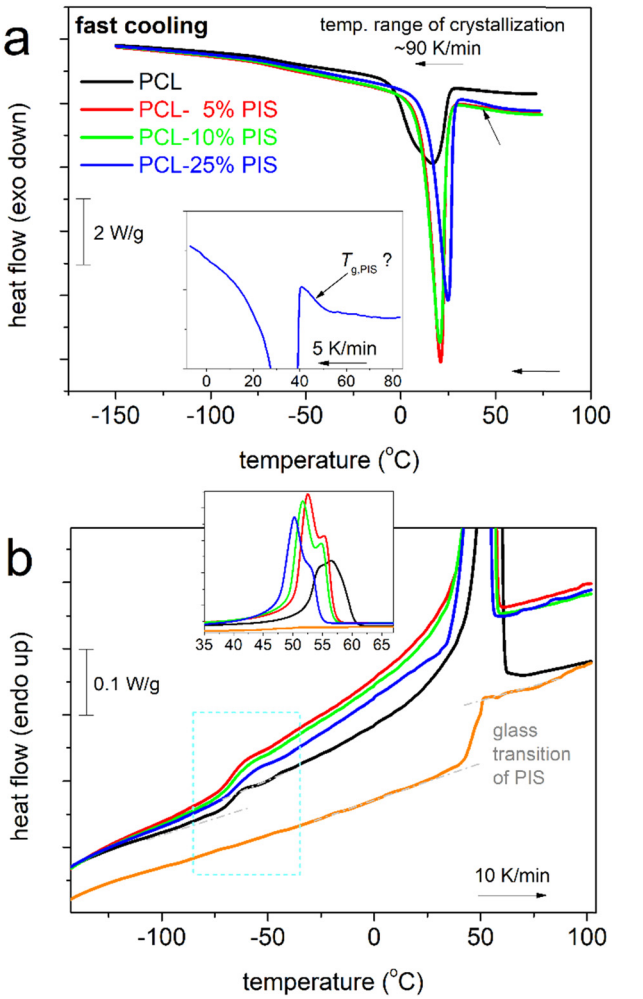

Fig. 5 Comparative DSC traces (a) during cooling at the highest achievable rate (~90 K min^{-1}) and (b) the subsequent heating at 10 K min^{-1} for all samples. The inset of (a) shows a cooling scan for PCL(75)/PIS(25) during cooling at 5 K min^{-1}, whereas the inset of (b) shows with better magnification the region of the melting of PCL crystals.

Recalling the results of neat PIS (T_g = 51 °C), the said step is most probably the individual glass transition of PIS in the copolymer. If so, PCL(75%)-*b*-PIS(25%) should be the only case of nano- or micro-phase separation within our copolymers. This phase separation is obviously more extensive when the amount of PIS is increased, as our materials are actually diblocks and PIS is not miscible with PCL. The same has been found true also in previous copolymers, based on other polyesters[76] of severely different T_gs and miscibilities, and shows that despite the chemical forced coexistence of different polymers, there are still physical mechanisms that drive the phase separation.

The results of the thermal transitions are quite similar when the samples are cooled at a higher rate (Fig. 5), with indications for weak cold crystallization upon heating slightly above T_g (Fig. 5b) probably due to incomplete crystallization during cooling.

To visualize the situation on semicrystalline morphology, *i.e.*, a term used to describe together the number(s)–size(s)–distributions(s) of the polymer crystallites, we employed POM. The results are shown in Fig. 6. The POM images are representative of all PCL-based systems, during crystallization from the melt. Please note that the thermal protocol employed for POM is similar to that of scan 2 in DSC, so that a comparison between the two techniques is facilitated. Within all compositions, spherulites are formed exhibiting similar sizes, varying between tens and hundreds μm. In all cases, the sample volume is finally filled with crystallites. The formation of small and larger crystals could possibly lay at the origins of the double-peaked melting recorded in DSC (insets to Fig. 3b and 5b).

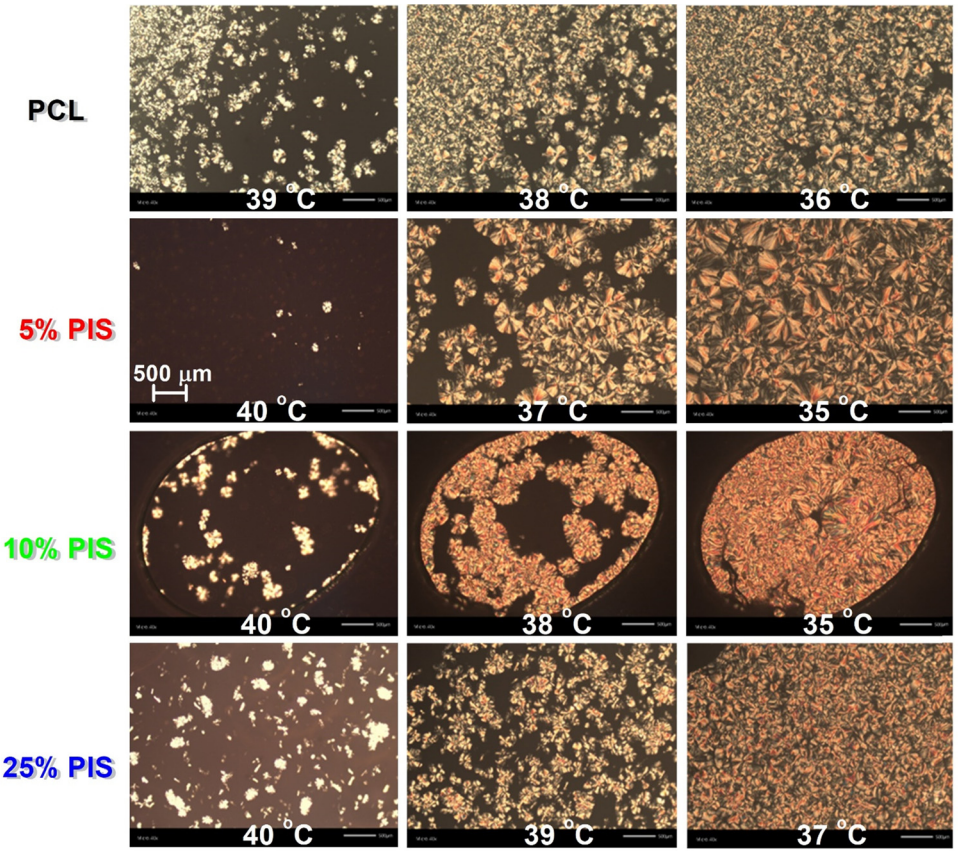

Fig. 6 Representative POM images for all PCL-based samples, during cooling from the melt state, results are shown at selected and indicated temperatures. For PCL(90%)-*b*-PIS(10%), the oval-shaped image is observed, differing from the other samples, which is due to the smaller amount employed for the said sample in POM (for technical reasons).

Regarding the effects of the copolymer composition on the semicrystalline morphology we do not observe systematic alternations. For example, on average larger crystals are formed in PCL(95%)-*b*-PIS(5%) and PCL(90%)-*b*-PIS(10%), whereas quite smaller ones are formed within PCL(75%)-*b*-PIS(25%), whereas, the latter samples demonstrates a view quite similar to that of neat PCL.

Regarding the quality of the spherulite structure, XRD measurements revealed interesting effects. In Fig. 7a, we present comparative XRD spectra for all samples, upon subjection to the same thermal/crystallization protocol. Neat PCL exhibits diffraction peaks originating from crystal forms, in accordance with the literature.[48] The corresponding 2θ positions are reported within Fig. 7a.

When comparing neat PCL with the PCL-*b*-PIS systems, the diffraction peaks for the latter are the same in number and appear broadly in the same 2θ range, but with migration toward lower 2θ by about 1°. The result has been checked by different samples and re-positionings of all samples and was found repeatable. This interesting effect suggests larger unit cells for the crystals of the copolymers or, from another point of view, it can be connected to looser lamella packing in the crystals.[48,78] These are compatible with the discussed effects on T_m in Fig. 4b. The effect on chain packing arises most probably from the presence of the more rigid PIS block. The first factor seems less possible. To support that, we present in Fig. 7b previously published XRD results[48] on neat PCL samples prepared by ROP by our group, characterized by a variety of molar masses, and subjected to a similar thermal treatment to that of the present study. Within these results, no significant migration of the diffraction peaks was observed.

Also, from the data of XRD and upon careful analysis in terms of mathematical models (Lorentzians, not shown here),[48] we estimated the crystalline fraction by the said technique, CF_{XRD}. The results have been shown in Fig. 4a and show quite good agreement with those on CF_c by DSC.

In the light of combined XRD (2θ changes) and DSC (lowering of T_m) effects on the probable looser lamella packing in the copolymers seems essential, however, at the same time, CF increases. An opposite behaviour would be expected in general; whereas, it has been observed before for complex systems, such as copolymers.[67,76,79] This non-trivial situation here, regarding crystallization, suggests that the mechanisms of chain-folding (lamellae) or/and the inter-chain interaction, probably also the nucleation, in the case of the present copolymers is different as compared to homopolymers.

In the case of PCL(75%)-*b*-PIS(25%) shown in Fig. 4a, the mismatch between CF_c and CF_{XRD} is worth noting. The mismatch seems to exist even when considering together the uncertainties in the estimation of CF_{XRD} (± 0.01) and CF_c (± 0.05). This could be,

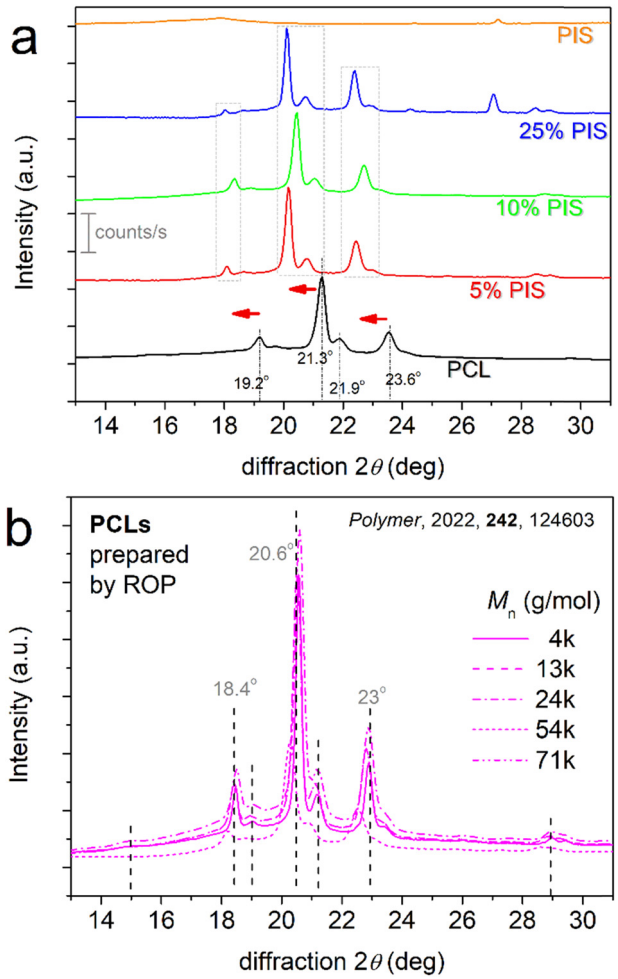

Fig. 7 (a) Comparative XRD spectra for PCL, PCL-PIS and initial PIS samples. Indicated are the main 2θ positions for the crystalline-related diffraction peaks, whereas horizontal red arrows have been added to point the effects induced in the copolymers. For comparison with the present systems, we show in (b) the results for neat PCLs prepared *via* ROP, characterized by a variety of M_n (adapted from Ref. 48 with permission from Elsevier).

in principle, due to the different techniques and the far different methods of calculation of crystalline fractions. Except for these, we should not ignore the presence of significant amounts of amorphous segments (PIS) in between the segments (PCL-rich) interfering in the crystallization process. Also, in some cases, XRD is known to be less sensitive in delicate/weak changes in crystallinity[80] (and references therein).

A final comment on XRD, refers to a diffraction peak recorded at 27.2° in neat PIS. A similar peak is recorded in PCL-25%PIS at 27.0°. The measurements have been repeated to check the recordings and the peaks were recorded again. The origin of these two peaks is unknown and mainly unexpected, as they seem to arise from PIS, which, is, nevertheless, amorphous. Unfortunately, we could not propose anything on the origin of the peak, since this is a relatively novel polymer, the available data in the literature are limited and there are no similar recordings for comparison.

At this point, we turn our attention to molecular mobility as studied by BDS. The results by BDS are discussed on the basis of the frequency, f, and temperature, T, dependence of ε'' (imaginary permittivity), which is related to the dielectric loss. In Fig. 8a and b, we present the raw results for neat PCL and initial PIS. Therein, we record in the form of $\varepsilon''(f)$ peaks the various types of dielectric relaxations, related directly to the relaxation times of the molecular groups. The relaxation processes are categorized into the local ones, recorded in general at temperatures below T_g, exhibiting low contributions to the permittivity and named with the Greek letters β, γ, *etc.*,[81,82] whereas, the segmental (large scale) ones, are recorded at $T \geq T_g$, named α.[82,83] The α relaxations are related to the glass transition and, as expected, contribute more strongly to the dielectric signal. In polymers, there is a qualitative difference between the glass transition as recorded by calorimetry (static) and by dynamical techniques (dynamic, α relaxation). However, the static glass transition is due to collective chain segment mobility with relaxation times of ~100 s, the dynamic α relaxation screens the molecular mobility of the chain, moreover, for various relaxation times (dynamics).[84,85] In some cases of polymers of relatively short chains, including PCL, another segmental-related process can be recorded, *i.e.*, the so-called Normal Mode.[86]

In neat PCL (Fig. 8a), at T between −150 and −50 °C, the γ_{PCL} and β_{PCL} relaxations are recorded, arising from the mobility of local PCL molecular groups. Examples of fitting (HN model, eqn 4) of all processes are presented in Fig. 9. γ_{PCL} has been proposed to originate on dipole moments arising from rotations (crankshaft-type) of the non-bound carbonyls on the PCL backbone.[81,87,88] Due to the latter, a connection of this local mobility with the segmental one is considered,[82] similarly to many other polyesters (lactide-, furan-, vanillate-based).[89–91] The connection is monitored, among others, *via* the sharp increase in its strength and changes in its overall time scale when T approaches T_g on heating (Fig. 8a). The time scale of γ_{PCL} has been found independent of M_n,[48] whereas it exhibits a general increase in magnitude, $\Delta\varepsilon$, with increasing M_n. The activation energy for γ_{PCL} is E_{act} = 0.36 eV. At higher temperatures/lower frequencies, the weaker β_{PCL} is recorded with E_{act} ~ 0.5 eV. β_{PCL} has been attributed to chain crankshaft motions in the amorphous and crystalline phase by Vanderschueren *et al.*[88] Grimau *et al.*[82] showed that the strength of β_{PCL} increases upon hydration whereas it is independent of M_n.[48] The relaxation has also been categorized as a process of the so-called Johari–Goldstein -type.[82,92] Finally, at around −60 °C, the segmental α_{PCL} relaxation enters our frequency window (Fig. 8a). In general, for all polymers, the relaxation arises from dipole moments perpendicular to the polymer chains, subsequently, it screens the cooperative motions of the polymer chains in the rubbery state.[69] The fragility of α_{PCL} was m_α = 75 (Table 2), denoting a weak level of chain–chain cooperativity, most probably due to the semicrystalline character of the polymer.[48,93,94] With the increase of temperature, α_{PCL} migrates fast to higher frequencies and the low-frequency becomes dominated by strong signal uptake, due to the

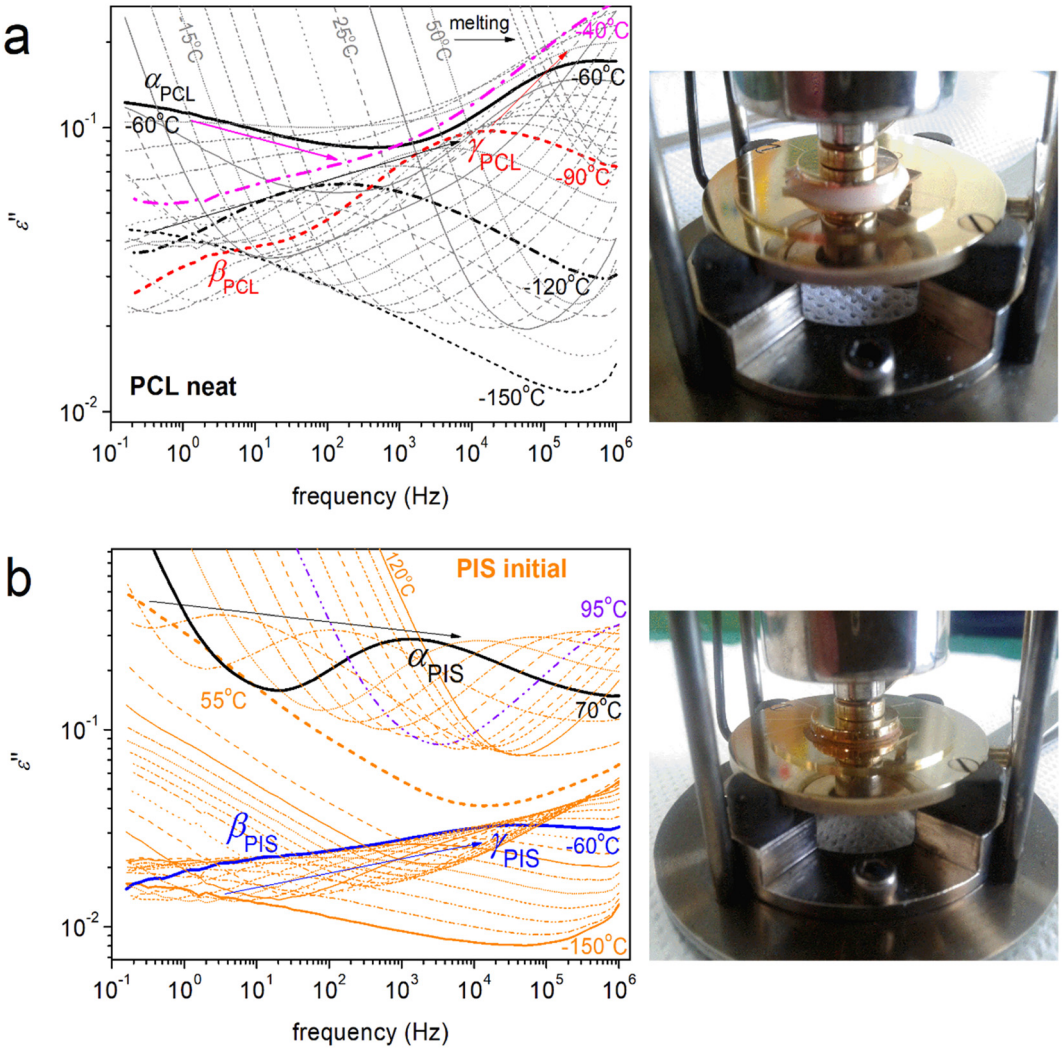

Fig. 8 Isothermal BDS plots (raw data) of the imaginary part of dielectric permittivity against frequency for (a) neat PCL and (b) initial PIS. Indicated are the main relaxation processes recorded at selected temperatures. On the right side, we show real images of the samples in the form of sandwich-like capacitors of well-defined geometries, employing silica spaces, placed in the BDS measurement cell.

involvement of strong effects related to ionic conductivity and interfacial charge effects.[69,95] Examples are shown in Section S1 ESI† (Fig. S2).

Regarding initial PIS, the $\varepsilon''(f, T)$ is presented in Fig. 8b. Please note that, in contrast to PCL, PIS is amorphous, whereas its dielectric relaxation spectra are shown here for the first time. Two local-like and one segmental relaxations are recorded within PIS. The faster relaxation is named here as γ_{PIS}, observed in a temperature range from −130 to −50 °C. γ_{PIS} could be fitted well with the symmetric HN term (eqn (4)) with $\alpha_{HN} \sim 0.2$–0.3 and $\beta_{HN} = 1$. The process exhibits an E_{act} equalling 0.43 eV. γ_{PIS} should monitor the most localized motion of PIS, however, due to the lack of similar data in the literature, we could not conclude its molecular origin. Following γ_{PIS}, the slower by ∼4 order of *f*-magnitude and slightly weaker β_{PIS} is recorded at temperatures from about −80 to −50 °C. β_{PIS} was fitted by a HN term with $\alpha_{HN} \sim 0.31$ and $\beta_{HN} = 1$ (Fig. 9). The E_{act} of β_{PIS} is relatively high, ∼0.8 eV, denoting a more 'difficult/rigid' relaxation of the corresponding molecular unit. β_{PIS} could possibly correlate with the coupled tetrahydrofuran rings of PIS, in part or in whole (Fig. 1). Finally, the strong segmental α_{PIS} is recorded at temperatures from 55 to 95 °C. α_{PIS} exhibits an asymmetric $\varepsilon''(f)$ peak, as expected for amorphous mobility.[69,96] The corresponding HN shape parameters are $\alpha_{HN} \sim 0.5$ and $\beta_{HN} = 0.65$. The fragility of α_{PIS} was estimated as $m_\alpha = 175$ (Table 2).

To directly assess the copolymer composition effects on molecular mobility, we present selected results in comparative isothermal $\varepsilon''(f)$ plots of Fig. 9. The same results are replotted as comparative isochronal $\varepsilon''(T)$ plots and shown in Fig. 10. This latter form of presentation enables a more direct comparison with the calorimetric data. Fig. 10a shows the isochronal $\varepsilon''(T)$ at the lowest frequency of measurement of ∼0.1 Hz, the excellent agreement and temperature coincidence of the calorimetric glass transition (step) with the dielectric one (α relaxation peak). The coincidence is due to low frequency which is comparable to the equivalent frequency of DSC ($10^{-2.8}$ Hz or else, relaxation

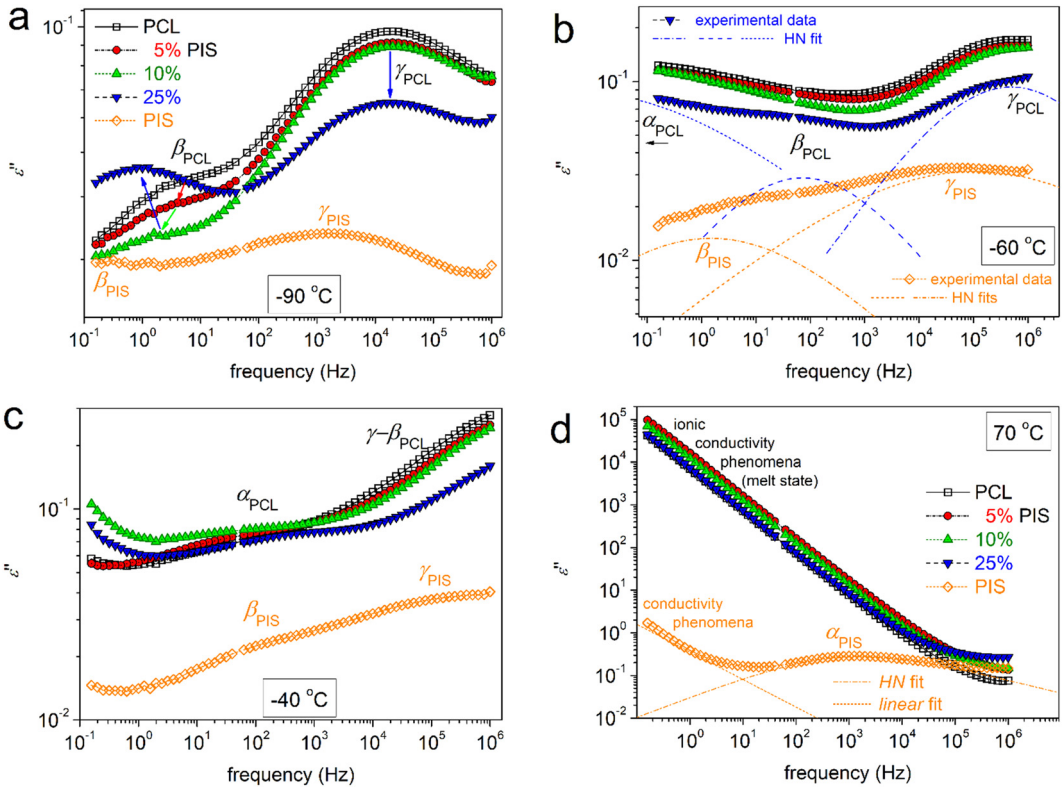

Fig. 9 Comparative isothermal BDS plots for the imaginary part of dielectric permittivity against frequency at the selected temperatures of (a) −90 °C, (b) −60 °C, (c) −40 °C and (d) 70 °C, for all samples. The recorded relaxation processes (peaks) are indicated on each plot. The added dash-dotted lines are fittings of the HN model to each ε″(*f*) peak.

Table 2 Values of interest by BDS on the segmental PCL relaxation. The estimated dielectric glass transition temeperature, $T_{g,diel}$, and the fragility index of α relaxation, m_α, the HN shape parameters, α_{HN} and β_{HN}, and representative values of the dielectric strength, $\Delta\varepsilon_\alpha$

	$T_{g,DSC}$ (°C)	$T_{g,diel}$ (°C)	m_α [a] (°C)	α_{HN} [b]	β_{HN}	$\Delta\varepsilon_\alpha$ [b]
PCL (neat)	−66	−54	75	∼0.30	1	0.6 → 0.3
PCL(95%)-*b*-PIS(5%)	−67	−56	69	∼0.28	1	1.0 → 0.6
PCL(90%)-*b*-PIS(10%)	−66	−62	63	∼0.30	1	1.0 → 0.4
PCL(75%)-*b*-PIS(25%)	−66	−65	62	∼0.26	1	0.9 → 0.6
PIS (initial)	51	52	175	0.52 → 0.47	∼0.65	1.4 → 2.2

[a] Refers to time scale of α relaxation upon stabilization of crystallization. [b] The arrows mark the effects recorded with increasing temperature.

time ∼100 s). In the said figures, we follow that, within the copolymers, the local and segmental relaxations of PCL dominate the signal, since the latter is the majority. However, it is interesting that the α_{PIS} relaxation cannot be resolved in the copolymers (Fig. 9d and 10). We recall results by DSC, in particular the insets to Fig. 3a and 5a, within which a glass transition step of PIS was recorded for PCL(75%)-*b*-PIS(25%). We can assume that the corresponding α_{PIS} relaxation is present here, however, is cloaked by the strong conductivity of PCL (Fig. 9d and 10). This is a strong indication that the PCL-phase is continuous throughout the whole sample volume for all copolymer compositions. This continuity is not disturbed by the PIS phase, which is glassy between for low *T*s and up to ∼50 °C.

This thus provides strong indications that the distribution of PCL and PIS is excellent for 5 and 10% PIS, whereas, for 25%PIS, PIS can be organized in nanodomains that are also well distributed within the copolymer volume. These data provide support for the successful synthesis of the copolymers, as in previous works on other co-polyesters,[58,67,76] while, from the methodological point of view, they prove the power of BDS as a tool for studying the structure–property relationship in polymers.

On the critical analysis of the complex spectra, shown in Fig. 9, we were able to construct the molecular mobility map that shows the time scale for all relaxations, in terms of the peak frequency maxima, $\log f_{max}$, against the inverse temperature, $1000/T$ (else called Arrhenius plots). These data are shown in Fig. 11.

In Fig. 11a, the different compositions of the copolymers does not seem to affect the time scale of γ_{PCL}, whereas, the addition of PIS leads to an acceleration of β_{PCL}. Neither of these relaxations is expected to change with M_n alternation.[48]

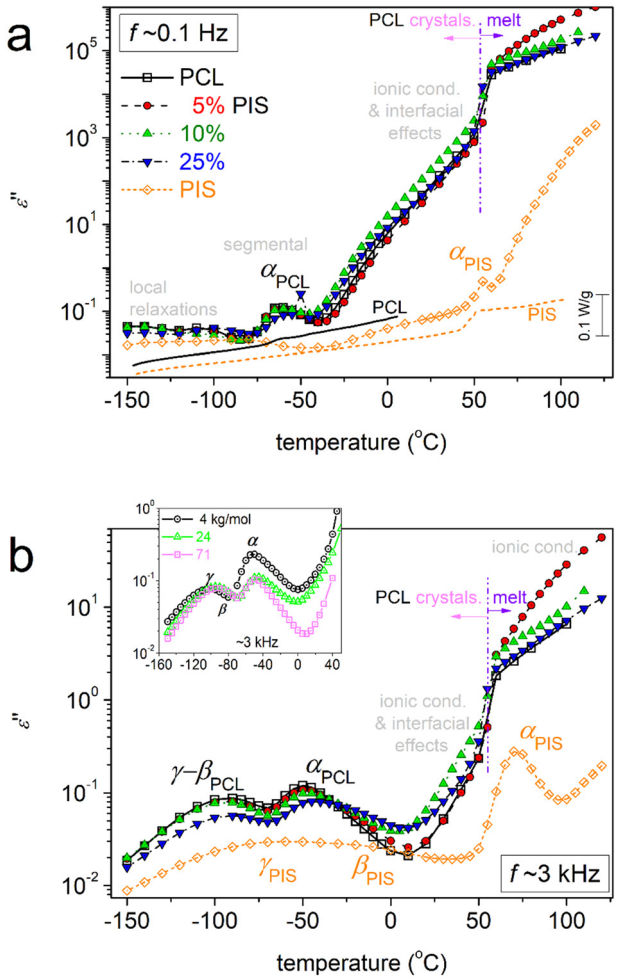

Fig. 10 Comparative isochronal curves of ε'' against temperature for all samples, indicated the main recorded relaxation processes (peaks of ε'') and the conductivity related phenomena at higher temperatures. The results are shown for two selected frequencies (a) ~0.1 Hz and (b) ~3 kHz. In (a), the BDS data (left axis) are directly compared with the calorimetric ones (right axis) for neat PCL and initial PIS. In the inset to (b) we compare with corresponding results on neat PCLs prepared by ROP for a wide range of M_ns (4–71 kg mol^{-1}) from a recent work by our group.[48]

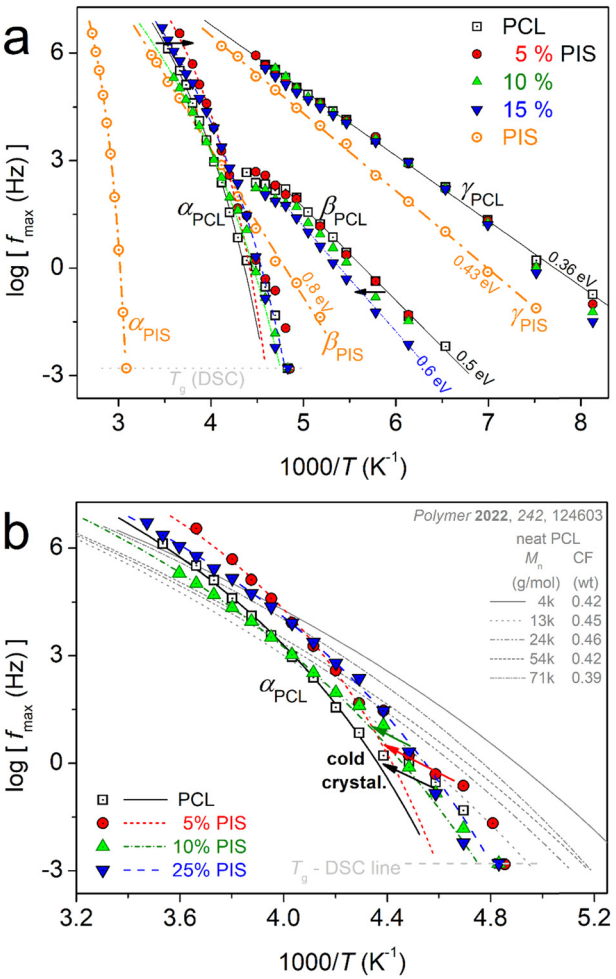

Fig. 11 Molecular mobility map (Arrhenius plots) for all samples, within (a) the overall temperature range and (b) focusing on the PCL segmental mobility (α_{PCL} relaxation). The added straight and curved lines connecting the experimental data points are fittings of the Arrhenius and Vogel–Fulcher–Tammann–Hesse equations. In (b, grey lines), we have added for comparison the results on neat PCL of various M_n, adapted from Ref. 48 with permission from Elsevier.

The acceleration of β_{PCL} is accompanied by systematic suppression of its strength, $\Delta\varepsilon$, from ~0.6 in PCL down to 0.2 in PCL(75%)-*b*-PIS(25%). At the same time, we recall the monotonic increase in CF (Fig. 4a). From that, we may conclude that β_{PCL} is activated within the amorphous PCL domains. The suppressed $\Delta\varepsilon$ should not be due to increased interchain interactions, as in such case its time scale would be in general hindered and that would be incompatible with the recorded acceleration of β_{PCL}.

The attention is now brought to segmental relaxation. Fig. 11b focuses on α_{PCL}. We recall that the BDS data are recorded isothermally at each T and at gradually increasing temperatures. As can be seen in Fig. 11b, during the initial temperatures (closer to T_g) the time scale points for α_{PCL} coincide well with the calorimetric T_g. As T increases, a disturbance-like change and a migration toward decelerated dynamics are recorded. This is due to the isothermal stay for some minutes at T where the polymer chains have become mobile (rubbery state) and most probably annealing of crystallization or additional cold crystallization take place.[48] Thus, crystal rearrangements[97,98] and/or additional growth is expected. This occurs in all cases of PCL-based samples. Please note that in DSC upon continuous heating, we have not recorded a significant exothermal event above T_g denoting cold crystallization. Among others this shows the high resolving power of BDS, being sensitive to such delicate polymer-phase changes.

So, only the experimental data for α_{PCL} upon completion of crystal annealing have been fitted to the VFTH model (eqn 6).[73] The fitting results are shown in Fig. 11b, as curved lines, which are characteristic of cooperative relaxations. The fitting involved the locking of the $f_{0,VFTH}$ parameter to the phonon frequency (10^{13} Hz).[69,99] From the extrapolation of these curves to

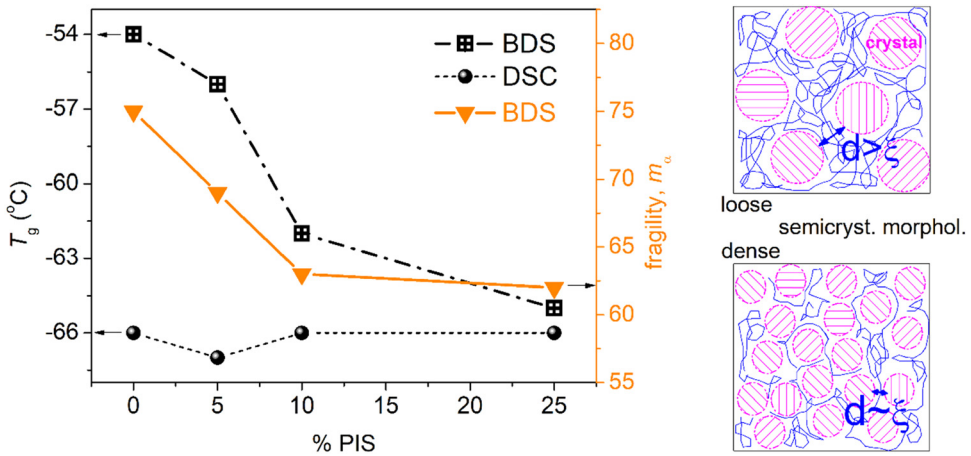

Fig. 12 (Left) The %PIS fraction dependence of (left axis) T_g as estimated by calorimetry and dielectric spectroscopy and (right axis) the estimated fragility of α relaxation. (Right) Simplified model scheme used to rationalize the effects on chain dynamics/cooperativity in terms of alternations in the semicrystalline morphology, subsequently, to the inter-crystal distances, *d*.

the equivalent frequency of conventional DSC ($f_{eq} \sim 10^{-2.8}$ Hz), we estimate the so-called 'dielectric glass transition temperature', $T_{g,diel}$. Also, from the evaluated fragility strength parameter of eqn 6, we calculated the fragility index, m_α,[99] which can be used as the measure of chains' cooperativity. The results on $T_{g,diel}$ and m_α are listed in Table 2 and are presented in comparison to the calorimetric T_g in Fig. 12.

In Fig. 12, we follow a monotonic decrease in $T_{g,diel}$ simultaneously with a decrease in m_α. Both results can be compatible with the shortening of the average chain length in the copolymers. However, we should always take into account the existence of an important crystalline fraction.

Coming back to Fig. 11b, therein, we compare the data of the present work with those of neat PCLs prepared by ROP and of various M_ns.[48] The latter results correspond again to semicrystalline PCLs of CFs from 0.39 to 0.46 wt.[48] Therein, with the exception of the lowest M_n (~4 kg mol^{-1}), the semicrystalline morphology was much denser as compared to the present PCL-based samples. As a result, the corresponding $T_{g,diel}$ as well as m_α had been recorded to be significantly smaller, namely, $T_{g,diel}$ between −71 and −80 °C and m_α between 39 and 42. These data have been interpreted in terms of systematic increasing effects of spatial nanoconfinement of the amorphous mobile chains between the PCL crystals.[48]

Adopting a similar scenario here, we propose that the decrease of $T_{g,diel}$ and m_α here, arises from spatial confinement of the chains between the crystals (milder compared to that of the previous work[48]). The said confinement is expected to arise from the formation of small/narrow amorphous polymer zones between the crystallites. To help the discussion, we visualized the situation by the scheme shown at the right side of Fig. 12. In order for the confinement to be effective, the average width, *d*, of these amorphous zones should be comparable to the chains' cooperativity length, ξ, namely, a few nm[48,83,100] (and references therein). Obviously, this cannot be checked by the present techniques. On the other hand, the effects of the expected decrease in M_n in the copolymers should be mainly indirect, *via* imposing direct effects on the rate and crystalline fraction. Except for the concept of crystals-related spatial confinement (scheme in Fig. 12), other complex scenarios could be employed to explain the dynamics situation. For example, special chain topology alternations in the copolymers and the existence of significant numbers of separated nano-phases, within which the constraints imposed on the polymer chains lead to suppression in the chain cooperativity. For the time being, only assumptions can be made, as these are quite delicate points that cannot be easily assessed by conventional techniques, especially when involving effects on the nanoscale. Small angle X-ray scattering (SAXS) could illuminate these aspect point[71,72] in the future.

Compatible to the aforementioned spatial confinement, may be the increase in the free volume[101] of the amorphous phase leads to the increase of the interchain distances. Such results could be interesting from the point of view of manipulating the air (oxygen) and water sorption, subsequently, to favour the compostability of our copolymers.

Such aspects as well as others referring, *e.g.*, to the mechanical performance and thermal conductivity can be illuminated in future work. Along these, an in-depth structural characterization of PCL-*b*-PIS copolymers and degradation studies are in progress and will be soon reported.

4. Conclusions

In this work, we investigated the molecular mobility and thermal transitions in novel PCL – PIS block copolymers, with semicrystalline PCL being the majority. Due to the latter, the properties of PCL were found to govern the final material properties, from local to segmental mobilities, ionic conductivity and crystallinity. The impact of PIS, an amorphous renewable polymer exhibiting high T_g, was found to be indirect, in the sense of contributing to the lowering of the PCL block length and facilitating a certain chain topology. As a result, the segmental mobility of PCL chains was found to accelerate,

demonstrating lower cooperativity. The mobility of PCL in the copolymers was found to be altered, in comparison to neat PCL (of various M_n values), and this again arises from the synthetic route. Subsequently, the indirect effects led to a moderately enhanced crystal nucleation and a worth noting increase in the crystalline fraction. On the other hand, compared with neat PCL, there are differences recorded in the structure of the crystals, consisting, for example, of looser lamellae. These outcomes are expected to play significant roles in the final properties of our materials, *e.g.*, on the mechanical performance, thermal conductivity, gases and small molecule permeation, compostability, *etc.*, that are exploitable within many applications regarding polymeric materials.[31,102,103] Such issues are worth studying in the future, considering the sustainable character of the said polymers. From the methodological point of view, in accordance with previous works on co-polyesters synthesized by similar strategies,[58,67,76] we showed that the combination of the employed techniques (BDS, DSC, *etc.*)[104] in addition to careful analysis of as many parameters as possible, is able to provide a structure/topology/inter-chain association view of complex polymeric materials that cannot be easily discerned *via* optical microscopy or other structure techniques. Moreover, once again, we conclude that implementing a synthetic strategy for co-polyesters is found to be successful regarding the achievement of homogeneous systems.

Author contributions

Chaima Bouyahya: investigation, formal analysis, resources, and writing – review and editing. Nikolaos D. Bikiaris: investigation, validation, and writing – review and editing. Alexandra Zamboulis: investigation, formal analysis, validation, and writing – review and editing. Apostolos Kyritsis: resources, validation, and writing – review and editing. Mustapha Majdoub: resources, validation, and writing – review and editing. Panagiotis A. Klonos: conceptualization, methodology, investigation, formal analysis, visualization, and writing – original draft.

Data availability

The raw/processed data required to reproduce these findings cannot be shared at this time due to technical or time limitations.

Conflicts of interest

There are no conflicts to declare.

Acknowledgements

This work was developed within the scope of the ERASMUS+ project between the University of Monastir and the Aristotle University of Thessaloniki. P. A. K. would like to thank Dr Daniel Fragiadakis (Naval Research Laboratory, Polymer Physics Section, Washington DSC, USA) for the provision of the sophisticated data analysis software 'Grafity' (**http://grafitylabs.com/**).

References

1 H. G. Elias, *An introduction to polymer science*, VCH, Weinheim, 1997.
2 M. Chanda and S. K. Roy, *Industrial polymers, specialty polymers, and their applications*, CRC Press, Boca Raton, 2008.
3 S. J. Rowan, *ACS Macro Lett.*, 2021, **10**, 466–468.
4 P. Pan and Y. Inoue, *Prog. Polym. Sci.*, 2009, **34**, 605–640.
5 A. Lendlein and A. Sisson, *Handbook of biodegradable polymers: isolation, synthesis, characterization and applications*, Wiley-VCH, Weinheim, Germany, 2011.
6 M. Tanaka, K. Sato, E. Kitakami, S. Kobayashi, T. Hoshiba and K. Fukushima, *Polym. J.*, 2015, **47**, 114–121.
7 L. Sisti, G. Totaro and P. Marchese, *PBS makes its entrance into the family of biobased plastics*, John Wiley & Sons, Hobocan, NJ, USA, 2016.
8 E. Balla, V. Daniilidis, G. Karlioti, T. Kalamas, M. Stefanidou, N. D. Bikiaris, A. Vlachopoulos, I. Koumentakou and D. N. Bikiaris, *Polymers*, 2021, **13**, 1822.
9 S. Saeidlou, M. A. Huneault, H. Li and C. B. Park, *Prog. Polym. Sci.*, 2012, **37**, 1657–1677.
10 I. Armentano, N. Bitinis, E. Fortunati, S. Mattioli, N. Rescignano, R. Verdejo, M. A. Lopez-Manchado and J. M. Kenny, *Prog. Polym. Sci.*, 2013, **38**, 1720–1747.
11 Y. Ikada and H. Tsuji, *Macromol. Rapid Commun.*, 2000, **21**, 117–132.
12 C. K. Williams, *Chem. Soc. Rev.*, 2007, **36**, 1573–1580.
13 M. Ebara, K. Uto, N. Idota, J. M. Hoffman and T. Aoyagi, *Soft Matter*, 2013, **9**, 3074–3080.
14 Y. Zhu, C. Romain and C. K. Williams, *Nature*, 2016, **540**, 354–362.
15 G. Z. Papageorgiou, *Polymers*, 2018, **10**, 952.
16 T. Fujimaki, *Polym. Degrad. Stab.*, 1998, **59**, 209–214.
17 M. Lahcini, H. Qayouh, T. Yashiro, P. Simon and H. R. Kricheldorf, *J. Macromol. Sci., Part A: Pure Appl.Chem.*, 2010, **47**, 503–509.
18 A. Zamboulis, E. A. Nakiou, E. Christodoulou, D. N. Bikiaris, E. Kontonasaki, L. Liverani and A. R. Boccaccini, *Int. J. Mol. Sci.*, 2019, **20**, 6210.
19 G. Z. Papageorgiou, D. G. Papageorgiou, Z. Terzopoulou and D. N. Bikiaris, *Eur. Polym. J.*, 2016, **83**, 202–229.
20 Z. Terzopoulou, L. Papadopoulos, A. Zamboulis, D. G. Papageorgiou, G. Z. Papageorgiou and D. N. Bikiaris, *Polymers*, 2020, **12**, 1209.
21 E. Xanthopoulou, Z. Terzopoulou, A. Zamboulis, L. Papadopoulos, K. Tsongas, D. Tzetzis, G. Z. Papageorgiou and D. N. Bikiaris, *ACS Sustainable Chem. Eng.*, 2021, **9**, 1383–1397.
22 M. Hong and E. Y. X. Chen, *Green Chem.*, 2017, **19**, 3692–3706.
23 W. Post, A. Susa, R. Blaauw, K. Molenveld and R. J. I. Knoop, *Polym. Rev.*, 2020, **60**, 359–388.
24 G. Rizis, T. G. van de Ven and A. Eisenberg, *Soft Matter*, 2014, **10**, 2825–2835.
25 I. Arandia, A. Mugica, M. Zubitur, R. Mincheva, P. Dubois, A. J. Müller and A. Alegría, *Macromolecules*, 2017, **50**, 1569–1578.

26 Y. Yu, Z. Wei, Y. Liu, Z. Hua, X. Leng and Y. Li, *Eur. Polym. J.*, 2018, **105**, 274–285.
27 M. Safari, A. Mugica, M. Zubitur, A. Martínez de Ilarduya, S. Muñoz-Guerra and A. J. Müller, *Polymers*, 2020, **12**, 17.
28 S. Nanaki, A. Viziridou, A. Zamboulis, M. Kostoglou, G. Z. Papageorgiou and D. N. Bikiaris, *Polymers*, 2020, **12**, 852.
29 J. M. Raquez, Y. Habibi, M. Murariu and P. Dubois, *Prog. Polym. Sci.*, 2013, **38**, 1504.
30 T. P. Gumede, A. S. Luyt and A. J. Müller, *eXPRESS Polym. Lett.*, 2018, **12**, 505–529.
31 L. Calandrelli, M. Annunziata, F. Della Ragione, P. Laurenzo, M. Malinconico and A. Oliva, *J. Mater. Sci.: Mater. Med.*, 2010, **21**, 2923–2936.
32 P. A. Klonos, M. Lazaridou, Ch Samiotaki, A. Kyritsis and D. N. Bikiaris, *Polymer*, 2022, **259**, 125329.
33 S. Fakirov, *Biodegradable polyesters*, JohnWiley & Sons, Auckland, *New Zealand*, 2015.
34 I. Manavitehrani, A. Fathi, H. Badr, S. Daly, A. Negahi Shirazi and F. Dehghani, *Polymers*, 2016, **8**, 20.
35 G. Fleche and M. Huchette, *Starch-Starke*, 1986, **38**, 26–30.
36 W. Fang, F. Xu, Y. Zhang, Z. Zhang, Z. Yang, W. Wang, H. He and Y. Luo, *Catal. Sci. Technol.*, 2022, **12**, 1756–1765.
37 S. Laanesoo, O. Bonjour, J. Parve, O. Parve, L. Matt, L. Vares and P. Jannasch, *Biomacromolecules*, 2021, **22**, 640–648.
38 L. Feng, W. Zhu, W. Zhou, C. Li, D. Zhang, Y. Xiao and L. Zheng, *Polym. Chem.*, 2015, **6**, 7470–7479.
39 Z. Terzopoulou, N. Kasmi, V. Tsanaktsis, N. Doulakas, D. N. Bikiaris, D. A. Achilias and G. Z. Papageorgiou, *Materials*, 2017, **10**, 801.
40 Y. Wang, C. J. E. Davey, K. van der Maas, R. J. van Putten, A. Tietema, J. R. Parsons and G. J. M. Gruter, *Sci. Total Environ.*, 2022, **815**, 152781.
41 N. Hammami, M. Majdoub and J. P. Habas, *Eur. Polym. J.*, 2017, **93**, 795–804.
42 N. Hammami, N. Jarroux, M. Robitzer, M. Majdoub and J. P. Habas, *Polymers*, 2016, **8**, 294.
43 S. Benali and P. Dubois, in *Environmental silicate nano-biocomposites, green energy and technology*, ed. L. Avérous and E. Pollet, Springer-Verlag, London, 2012, ch. 5, p. 119.
44 L. N. Woodard and M. A. Grunlan, *ACS Macro Lett.*, 2018, **7**, 976–982.
45 A. C. Albertsson, *Adv. Polym. Sci.*, 2002, **157**, 1–179.
46 Y. Wang, B. Liu, X. Wang, W. Zhao, D. Liu, X. Liu and D. Cui, *Polym. Chem.*, 2014, **5**, 4580–4588.
47 M. C. Righetti, *Materials*, 2017, **10**, 442.
48 P. A. Klonos, N. D. Bikiaris, E. Christodoulou, A. Zamboulis, G. Z. Papageorgiou and A. Kyritsis, *Polymer*, 2022, **242**, 124603.
49 J. Lin, S. Shenogin and S. Nazarenko, *Polymer*, 2002, **43**, 4733–4743.
50 P. A. Klonos, S. N. Tegopoulos, C. S. Koutsiara, E. Kontou, P. Pissis and A. Kyritsis, *Soft Matter*, 2019, **18**, 1813–1824.
51 P. A. Klonos, V. Peoglos, D. N. Bikiaris and A. Kyritsis, *J. Phys. Chem. C*, 2020, **123**, 5469–5479.
52 A. Toda, R. Androsch and C. Schick, *Polymer*, 2016, **91**, 239–263.
53 A. Wurm, E. Zhuravlev, K. Eckstein, D. Jehnichen, D. Pospiech, R. Androsch, B. Wunderlich and C. Schick, *Macromolecules*, 2012, **45**, 3816–3828.
54 R. A. Pérez, M. E. Córdova, J. V. López, J. N. Hoskins, B. Zhang, S. M. Grayson and A. J. Müller, *React. Funct. Polym.*, 2014, **80**, 71–82.
55 L. Sangroniz, R. G. Alamo, D. Cavallo, A. Santamaría, A. J. Müller and A. Alegría, *Macromolecules*, 2018, **51**, 3663–3671.
56 J. Wang, M. K. Cheung and Y. Mi, *Polymer*, 2002, **43**, 1357–1364.
57 M. F. Koenig and S. J. Huang, *Polymer*, 1995, **36**, 1877–1882.
58 E. Christodoulou, P. A. Klonos, K. Tsachouridis, A. Zamboulis, A. Kyritsis and D. N. Bikiaris, *Soft Matter*, 2020, **16**, 8187–8201.
59 P. B. Messersmith and E. P. Giannelis, *J. Polym. Sci., Part A: Polym. Chem.*, 1995, **33**, 1047–1057.
60 D. J. A. Cameron and M. P. Shaver, *Chem. Soc. Rev.*, 2011, **40**, 1761–1776.
61 H. Zhang and M. W. Grinstaff, *Macromol. Rapid Commun.*, 2014, **35**, 1906–1924.
62 S. G. Nanaki, G. Z. Papageorgiou and D. N. Bikiaris, *J. Therm. Anal. Calorim.*, 2012, **108**, 633–645.
63 A. Schönhals and P. Szymoniak, *Dynamics of composite materials*, Springer, Cham, Switzerland, 2022.
64 M. A. Woodruff and D. W. Hutmacher, *Prog. Polym. Sci.*, 2010, **35**, 1217–1256.
65 E. Roumeli, D. G. Papageorgiou, V. Tsanaktsis, Z. Terzopoulou, K. Chrissafis, A. Avgeropoulos and D. Bikiaris, *ACS Appl. Mater. Interfaces*, 2015, **7**, 11683–11694.
66 Z. Terzopoulou, A. Zamboulis, D. N. Bikiaris, M. A. Valera and A. Mangas, *Polymers*, 2021, **13**, 4121.
67 V. Karava, A. Siamidi, M. Vlachou, E. Christodoulou, A. Zamboulis, D. N. Bikiaris, A. Kyritsis and P. A. Klonos, *Soft Matter*, 2021, **17**, 2439–2453.
68 V. Crescenzi, G. Manzini, G. Calzolari and C. Borri, *Eur. Polym. J.*, 1972, **8**, 449–463.
69 F. Kremer and F. Schönhals, *Broadband dielectric spectroscopy*, Springer-Verlag, Berlin, 2002.
70 G. P. Baeza, C. Dessi, S. Constanzo, D. Zhao, S. Gong, A. Alegria, R. H. Colby, M. Rubinstein, D. Vlassopoulos and S. K. Kumar, *Nat. Commun.*, 2016, **7**, 11368.
71 A. C. Genix, V. Bocharova, B. Carroll, M. Lehmann, T. Saito, S. Krueger, L. He, P. Dieudonné-George, A. P. Sokolov and J. Oberdisse, *ACS Appl. Mater. Interfaces*, 2019, **11**, 17863–17872.
72 A. P. Holt, P. J. Griffin, V. BOcharova, A. L. Agapov, A. E. Imel, M. D. Dadmun, J. R. Sangoro and A. P. Sokolov, *Macromolecules*, 2014, **47**, 1837–1843.
73 R. Boehmer, K. Ngai, C. A. Angell and D. J. Plazek, *J. Chem. Phys.*, 1993, **99**, 4201–4209.
74 S. Koutsoumpis, A. Poulakis, P. Klonos, S. Kripotou, V. Tsanaktsis, D. N. Bikiaris, A. Kyritsis and P. Pissis, *Thermochim. Acta*, 2018, **666**, 229–240.
75 A. De Almeida, M. Nébouy and P. Baeza, *Macromolecules*, 2019, **52**, 1227–1240.
76 P. A. Klonos, Z. Terzopoulou, A. Zamboulis, M. A. Valera, A. Mangas, A. Kyritsis, P. Pissis and D. N. Bikiaris, *Soft Matter*, 2022, **18**, 3725–3737.

77 M. E. Córdova, A. T. Lorenzo, A. J. Müller, J. N. Hoskins and S. M. Grayson, *Macromolecules*, 2011, **44**, 1742–1746.
78 M. S. S. B. Monteiro, F. V. Chávez, P. J. Sebastião and M. I. B. Tavares, *Polym. Test.*, 2013, **32**, 553–566.
79 L. Papadopoulos, P. A. Klonos, M. Kluge, A. Zamboulis, Z. Terzopoulou, D. Kourtidou, A. Magaziotis, K. Chrissafis, A. Kyritsis, D. N. Bikiaris and T. Robert, *Polym. Chem.*, 2021, **12**, 5518–5534.
80 M. Doumeng, L. Makhlouf, F. Berthet, O. Marsan, K. Delbé and F. Chabert, *Polym. Test.*, 2021, **93**, 106878.
81 R. Sabater i Serra, J. L. Escobar Ivirico, J. M. Meseguer Dueñas, A. Andrio Balado, J. L. Gómez Ribeller and M. Salmerón Sánchez, *Eur. Phys. J. E: Soft Matter Biol. Phys.*, 2007, **22**, 293–302.
82 M. Grimau, E. Laredo, Y. M. C. Pérez and A. Bello, *J. Chem. Phys.*, 2001, **114**, 6417–6425.
83 Y. Suzuki, H. Duran, W. Akram, M. Steinhart, G. Floudas and H. J. Butt, *Soft Matter*, 2013, **9**, 9189–9198.
84 J. Hintermeyer, A. Herrmann, R. Kahlau, C. Goiceanu and E. A. Rössler, *Macromolecules*, 2008, **41**, 9335–9344.
85 A. Alegría, E. Guerrica-Echevarría, L. Goitiandía, I. Tellería and J. Colmenero, *Macromolecules*, 1995, **28**, 1516–1527.
86 O. Urakawa, K. Adachi, T. Kotaka, Y. Takemoto and H. Yasuda, *Macromolecules*, 1994, **27**, 7410–7414.
87 K. A. Masser, H. Yuan, A. Karim and C. R. Snyder, *Macromolecules*, 2013, **46**, 2235–2240.
88 J. Vanderschueren, M. Ladang and J. M. Heuschen, *Macromolecules*, 1980, **13**, 973–977.
89 P. A. Klonos, D. N. Bikiaris and A. Kyritsis, in *Dynamics of composite materials*, ed. A. Schönhals and P. Szymoniak, Springer, Cham, 2022, pp. 87–121.
90 E. Xanthopoulou, P. A. Klonos, A. Zamboulis, Z. Terzopoulou, A. Kyritsis, P. Pissis, D. N. Bikiaris and G. Z. Papageorgiou, *Polymer*, 2021, **233**, 124197.
91 D. Kourtidou, P. A. Klonos, L. Papadopoulos, A. Kyritsis, D. N. Bikiaris and C. Chrissafis, *Soft Matter*, 2021, **17**, 5815–5828.
92 G. P. Johari and M. Goldstein, *J. Chem. Phys.*, 1970, **53**, 2372.
93 H. Papananou, E. Perivolari, K. Chrissopoulou and S. Anastasiadis, *Polymer*, 2018, **157**, 111–121.
94 P. A. Klonos, L. Papadopoulos, M. Kasimatis, H. Iatrou, A. Kyritsis and D. N. Bikiaris, *Macromolecules*, 2021, **54**, 1106–1119.
95 R. Richert, A. Agapov and A. P. Sokolov, *J. Chem. Phys.*, 2011, **134**, 104508.
96 R. Lund, A. Alegría, L. Goitandia, J. Colmenero, M. A. Gonzalez and P. Lindner, *Macromolecules*, 2008, **41**, 1364–1376.
97 A. S. Altorbaq, A. A. Krauskopf, X. Wen, R. A. Pérez-Camargo, Y. Su, D. Wang, A. J. Müller and S. K. Kumar, *Prog. Polym. Sci.*, 2022, **128**, 101527.
98 K. Bornani, N. F. Mendez, A. S. Altorbaq, A. J. Müller, Y. Lin, E. Z. Qu, K. Zhang, S. K. Kumar and L. S. Schadler, *ACS Macro Lett.*, 2022, **11**, 818–824.
99 D. Fragiadakis, P. Pissis and L. Bokobza, *Polymer*, 2005, **46**, 6001.
100 A. Schönhals, H. Goering, C. Schick, M. Frick, M. Mayorova and R. Zorn, *Eur. Phys. J.: Spec. Top.*, 2007, **141**, 255–259.
101 R. M. Hodge, T. J. Bastow, G. H. Edward, G. P. Simon and A. J. Hill, *Macromolecules*, 1996, **29**, 8137–8143.
102 C. Pandis, S. Trujillo, M. Roganowicz and J. L. Gómez Ribelles, *Macromol. Symp.*, 2014, **341**, 34–44.
103 S. G. Nanaki, K. Pantopoulos and D. N. Bikiaris, *Int. J. Nanomed.*, 2011, **6**, 2981–2995.
104 P. Szymoniak, X. Qu, M. Abbasi, B. R. Pauw, S. Henning, Z. Li, D. Y. Wang, C. Schick, K. Saalwächter and A. Schönhals, *Soft Matter*, 2021, **17**, 2775–2790.

